Ultrasonic Ice Protection Systems: Analytical and Numerical Models for Architecture Tradeoff — Source link ↗

Marc Budinger, Valérie Pommier-Budinger, Gael Napias, Arthur Costa da Silva

Institutions: University of Toulouse, Institut supérieur de l'aéronautique et de l'espace

Related papers:

- Instantaneous De-Icing of Freezer Ice via Ultrasonic Actuation

- Ultrasonic de-icing of wind-tunnel impact icing

- Piezoelectric transducer actuated leading edge de-icing with simultaneous shear and impulse forces

- Mechatronic Development of Self-Actuating In-Flight Deicing Structures

- Delamination of surface accretions with structural waves: Piezo-actuation and power requirements

Ultrasonic ice protection systems: analytical and numerical models for architecture trade-off

Marc Budinger[(1)], Valérie Pommier-Budinger[(2)], Gael Napias[(2)], Arthur Costa Da Silva[(2)]

(1) INSA Toulouse, Institut Clément Ader, Toulouse, 31077, France

(2) ISAE SUPAERO, Institut Supérieur de l'Aéronautique et de l'Espace, 31055, France

ABSTRACT

Protection systems against ice conventionally use thermal, pneumatic or electro-thermal solutions. However, they are characterized by high energy consumption. This article focuses on low-consumption electromechanical deicing solutions based on piezoelectric transducers. After a review of the state of the art to identify the main features of electromechanical de-icing devices, piezoelectric transducer-based architectures are studied. Analytical models validated by numerical simulations allow trend studies to be performed which highlight the resonance modes and the ultrasonic frequency ranges that lead to low-consumption, compact ultrasonic deicing devices. Finally, de-icing systems widely studied with bonded ceramics and de-icing systems less usual with Langevin pre-stressed piezoelectric transducers are compared and a Langevin piezoelectric transducer-based device leading to an interesting compromise is tested.

Keywords: de-icing systems, electromechanical actuator, ultrasonic actuator, piezoelectric transducer, pre-stressed Langevin actuator

1. INTRODUCTION AND STATE OF THE ART

1.1. Ice protection systems

Ice accretion on aircraft has been a well identified problem since the beginning of the 20th century. It can lead to decreased lift, increased drag, reduced thrust reduction, and risk of stalling or even engine failure owing to ice ingestion. Icing occurs both during flight and on the ground. It has led to many aviation accidents, such as the Air Florida Boeing B737 (1982), the American Eagle ATR 72 (1997), and the Air France Airbus A330 (2009). To ensure aircraft safety, regulatory agencies, such as the CAA (Civil Aviation Authority [1]) and the FAA (Federal Aviation Administration [3]), have established regulations for aircraft anti-icing and de-icing.

Current strategies for anti-icing and de-icing [1] can be chemical, thermal or mechanical - each having different degrees of efficiency or environmental impact. The chemicals used for de-icing (ethylene, propylene glycol or diethylene glycol) can lower the freezing point but require large volumes of fluids and induce environmental issues and premature wear of the treated parts (especially corrosion). Thermal techniques are used for anti-icing and de-icing in flight and on the ground by liquefaction and vaporization of the ice, but require either a large amount of hot air under pressure to be bled from the engine or a large amount of energy to be provided by the electric grid for electro-thermal solutions. Thermal solutions require around 4 kW/m² and the total amount of power required to de-ice a Boeing 787 with an electrical de-icing system has been estimated at 76 kW [11]. Mechanical de-icing systems are low-energy solutions that aim to break the accumulated ice by applying a mechanical pulse or vibrations to the structure to be protected. Pneumatic systems are commonly used for their low cost but have a significant impact on the aerodynamics of the aircraft and require maintenance. Recent efforts to develop electromechanical systems are justified by the potential of such systems in terms of weight, durability and energy savings.

1.2. Electromechanical de-icing systems

Electromechanical deicing systems use electromagnetic actuators, piezoelectric actuators or shape memory alloys. These systems are presented in [1] and [6] and their advantages and drawbacks are analyzed in Table 1. This article focuses on actuation with piezoelectric technology, and especially on resonant piezoelectric technologies, which have a better power/mass ratio than static solutions. The deeper insight into piezoelectric de-icing systems presented in Table 2 allows a more detailed analysis to be carried out according to the frequency range of the modes activated by the piezoelectric actuators and to the type of piezoelectric actuators.

Ramanathan et al. [7] proposed the use of ultrasonic shear waves at very high frequency (1 MHz). They performed experiments with piezoelectric patches bonded to an isotropic plate with a layer of ice. The results indicate that the actuators were able to de-ice the aluminum plate by melting the ice at the interface. Kalkowski et al. [8] analyzed the frequency range for which wave-based technologies efficiently promote the delamination of ice with minimum power requirements.

Venna et al. [9][10][11][12] used piezoelectric ceramics bonded onto plates and on the inner flat surface of a leading edge structure to excite low frequency modes to delaminate ice (below 1000 Hz). They used analytical and numerical

models to identify the first modes for which the shear stress produced in the ice was greater than the shear stress that would theoretically lead to delamination. The average de-icing time varied between 46 s and 280 s and increased as the icing temperature decreased. Palacios [13] analyzed this result and found that the de-icing time seemed to show that the de-icing was more probably caused by thermal effects than by shear stress. S. Struggl et al. [14] conducted the same kind of analysis and experiments with piezoelectric ceramics bonded to a plate and on a leading edge structure to excite low frequency modes (below 500 Hz). They also performed tests in an icing research tunnel and the de-icing was successful at a frequency of 307 Hz.

Seppings [15] used a stack of thin piezo-electric discs held in compression by a bolt running through the center of the stack and showed that the pre-stressed actuator driven at 20 kHz was more efficient than piezoelectric patches.

Palacios initiated many studies on de-icing systems [16][17][18][19][20][21] and tested several technologies. For piezoelectric de-icing systems, he used piezoelectric patches to generate ultrasonic shear stress at high frequency (around a few tens of kHz). He performed tests on plates [16][17] and on leading edges [18]. At such frequencies, the delamination of the ice was instantaneous. He also tested an original design of a shear tube actuator driven at 300 V and 436 Hz [19]. In [20], experiments showed two main failures related to the bonding of the actuators: fracture of the piezoelectric ceramic at the solder joint location and delamination between the ceramic and the host. To tackle this problem, Palacios proposed optimizing the bonding of the supply wire on the ceramic and the bonding between the piezoelectric actuators and the substrate to avoid concentrations of stresses [21]. In [22], he also investigated the effect of hydrophobic coating combined with an ultrasonic deicing system and showed that the ice adhesion depended on the substrate roughness.

More recently, Strobl [23] used multilayer piezoelectric patches at frequencies around 4 kHz and icephobic coating to delaminate ice instantaneously on polished surfaces with a low supply voltage.

Technological solutions	Main advantages	Main drawbacks
Electromagnetic	Contactless possible, high displacements possible	Low force density, electromagnetic pollution, size of feeding electronics
Piezoelectric (PZT)	Force generation (good force/mass ratio) even at high frequency, energy consumption	Brittleness, small displacements
Shape Memory Alloy (SMA)	Force generation in static	Low dynamics, response time, energy consumption

Table 1 – Comparison of electromechanical deicing systems

Comparison criteria	Technological solutions	Previous works	Main advantages	Main drawbacks
Frequency range	Static, Low Frequency (Hz)	[9][10][11][12] [14]	Power supply	Force of activation
	Vibration (kHz)	[16][17] [18][19][20][21] [22][23]		Fatigue
	Waves (MHz)	[7][8]		Energy consumption
Technology	Bonded Piezoelectric ceramics (PZT or multilayers)	[9][10][11][12][15] [16][17][18] [20][21][21][22][14][23]	Easy to implement	Brittle Not easily adaptable to curved surfaces
	Pre-stressed piezoelectric transducer	[15]	Less brittle, stress-resistant	Frequency linked to the size of the transducer

Table 2 – Comparison of piezoelectric de-icing systems

1.3. Review of previous works, proposed architecture and objectives of present work

According to the previous analyses, the main features of piezoelectric de-icing devices are as follows:

- As regards the frequency range, previous studies on piezoelectric de-icing devices have shown that both low frequencies and ultrasonic high frequencies can be excited to generate shear stress and to break ice. However, no studies have been carried out to determine the best frequency range for which structural resonances maximize the shear stress in the ice while minimizing the stress in the substrate and in the actuators. Consequently, a specific study to determine the optimized frequency range is required and is proposed in this article.

- One other issue is the nature of the modes to be excited: both flexural and extensional modes can produce shear stress in a structure. Thus, a specific study to determine the kind of modes that produce maximal shear stress will be useful for the design of the de-icing system architecture.

- Regarding the actuation technology, this article will compare non-pre-stressed piezoelectric transducers (bonded ceramics) and pre-stressed piezoelectric transducers (Langevin transducer) in terms of force-to-density ratio, robustness, ease of integration in a curved leading edge and power consumption. Non-pre-stressed piezoelectric transducers have been widely tested and examples off architectures can be found in [9][15][16][18][23]. Figure 1 shows two different architectures with a pre-stressed piezoelectric actuator, one exciting flexural modes, the other exciting extensional modes. Both architectures lead to shear stress at the ice/substrate interface.
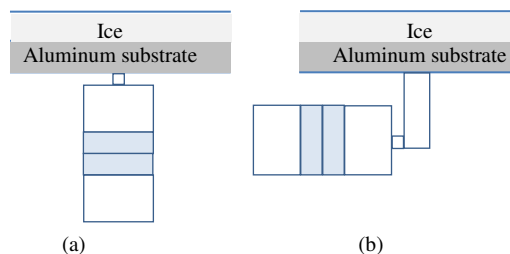
Figure 1 - Architecture for a de-icing system with a pre-stressed piezoelectric transducer: (a) Excitation of flexural modes, (b) Excitation of extensional modes

The objectives of this paper are thus:

- to develop analytical models validated by numerical simulations and complemented by measurements in order to perform trend studies highlighting the nature of the resonance modes and the frequency ranges leading to low-consumption, compact piezoelectric de-icing devices.

- to compare piezoelectric transducer-based architectures enabling an interesting compromise to be reached to generate shear stress at the ice/substrate interface and to promote ice delamination and cracking without damaging the actuator or the substrate.

2. FEASIBILITY OF PIEZOELECTRIC DE-ICING SYSTEMS BASED ON STRESS ANALYSIS

2.1. Study case

In this article, the study case is a simple plane rectangular plate of dimensions $290 \times 200 \times 1.5$ mm^3 that is covered by a 2mm thick layer of ice. The panels of an aircraft airframe are usually supported by ribs and stiffeners and the boundary conditions of such panels are close to clamped on all sides. However, the plates will be studied in the pinned boundary condition in this section because this condition enables simple analytical expressions to be formulated to estimate the stresses produced at the ice/substrate interface and because, at the high frequencies used in the study, the deformations in the middle of the plate are similar for pinned and clamped boundary conditions (as illustrated in Figure 2).

f = 12 254 Hz
Clamped boundary case

f = 11 434 Hz
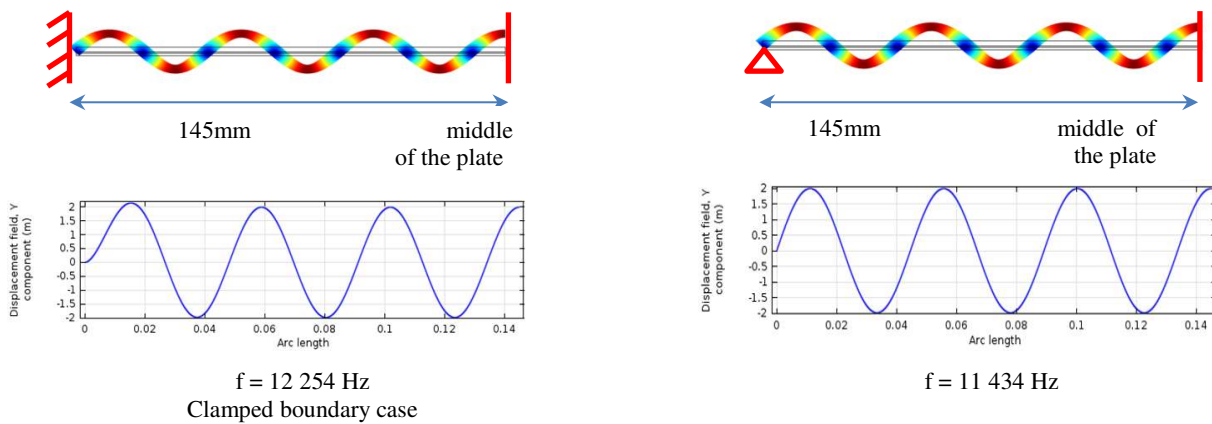
Figure 2 - Comparison of two boundary conditions (clamped versus pinned) for the study of a plate at high frequencies: displacements in the middle of the plate are sinusoidal in both cases

The mechanical properties of the ice considered for calculation were chosen so as to correspond to glaze ice and were selected among the values presented in [24]. The ice and aluminum mechanical properties used for the analyses performed in this article are shown in Table 3.

Material	Aluminum	Ice
E (GPa)	70	9.7
G (GPa)	26	3.7
ν $(-)$	0.33	0.30
ρ (kg/m^3)	2770	880

Table 3 –Mechanical properties of the study case materials

2.2. Stress generation

In order to choose the vibration modes that are the most suitable for de-icing by generation of stresses in a plate, four types of "failure" modes of the ice/substrate interface were considered: failure owing to excessive tensile stress; failure owing to excessive in-plane shear stress; failure owing to excessive out-of-plane shear stress and failure owing to excessive out-of-plane tensile stress. Figure 3 shows a simplified scheme of the mechanisms and the interface failure expected in each case. The values of ice strength are discussed in [25],[26],[27]. The parametric studies carried out by Scavuzzo et al. [25] and by Jellinek [26] and the experiments performed by Laforte et al. [27] indicate that the adhesion strength of ice depends mainly on the roughness of the accretion surface. Scavuzzos's study also suggests that the adhesion resistance to an out-of-plane stress (shear or tensile) depends, but to a lesser degree, on droplet momentum and surface temperature. Laforte's work shows that the adhesion resistance to an in-plane deformation (distortion or elongation) varies with the ice thickness and Loughborough observed dependence of the strength on the nature of the substrate [28]. Finally, Table 4 exposes the values of the properties presented in the references discussed. In this study, the targeted application is the de-icing of aircraft flight control surfaces. For this kind of application, ice delamination by shear is more efficient than breaking by tensile stress. This is why we focus on out-of-plane shear stress generation. For the assessment of the different de-icing system architectures, we will compute the out-of-plane shear stress and ice will be assumed to be de-bonded when the out-of-plane shear stress exceeds the critical adhesive strength of ice (considered to be 1 MPa for numerical applications of this paper). Moreover, to assess de-icing systems, the stress induced in the substrate and in the piezoelectric ceramics will also be computed in order to quantify the risk of damage to the ceramics.
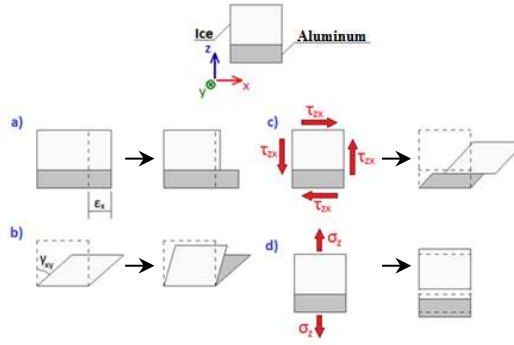
Figure 3 - Modes of failure of the ice-aluminum interface. a) Failure due to excessive in-plane tensile stress. b) Failure due to excessive in-plane shear stress. c) Failure due to out-of-plane shear stress. d) Failure due to excessive out-of-plane tensile stress

Ice Thickness (mm)	2	5	10
De-icing Tensile Strain $\epsilon_{x,crit}$ (μm/m)	500	420	280
De-icing In-Plane Shear Strain $\epsilon_{xy,crit}$ (μm/m)	700	350	212
De-icing Out-of-Plane Shear Stress $\tau_{zx,crit}$ (MPa)	1.10 – 0.55		
De-icing Out-of-Plane Tensile Stress $\sigma_{z,crit}$ (MPa)	1.20 – 0.95		
Ice Tensile Strength (MPa)	3.1 – 0.7		
Ice Compressive Strength (MPa)	5-25		
Ice Shear Strength (MPa)	0.7		

Table 4 –Adhesion properties of impact ice to aluminum surface with matte finish and its strength properties ([25],[26],[27])

2.3. Comparison of resonance modes on 1D models

The plate resonance modes used in the literature (section 1.2) are essentially in-plane extensional modes and out-of-plane flexural modes. They generate stress corresponding to failure modes a) and c) in Figure 3. However, piezoelectric actuators have limited displacement capacity. Consequently the comparison of these modes is made here in terms of stresses generated for a given displacement. To simplify the analysis, several assumptions are used: support and ice are

considered as a thin multilayer beam (1D model), mode shapes are assumed to be identical to those of a uniform beam and boundary conditions are simply supported as introduced in section 2.1. Figure 4 shows the beam under study where:

- x is the transverse position along the beam of length a ;

- n is the number of anti-nodes for the mode considered;

- ω is the pulsation of the mode considered;

- h_{alu}, h_{ice}, h_n are respectively the thickness of the aluminum beam, the thickness of the ice beam and the position of the neutral line for the flexural mode,

- $U(x)$ and $W(x)$ are respectively the in-plane displacements (for extensional modes) and out-of-plane displacements (for flexural modes);

- c_{alu} , c_{ice} , ρ_{alu} and ρ_{ice} are respectively the Young modulus and the density for the aluminum beam and the ice.
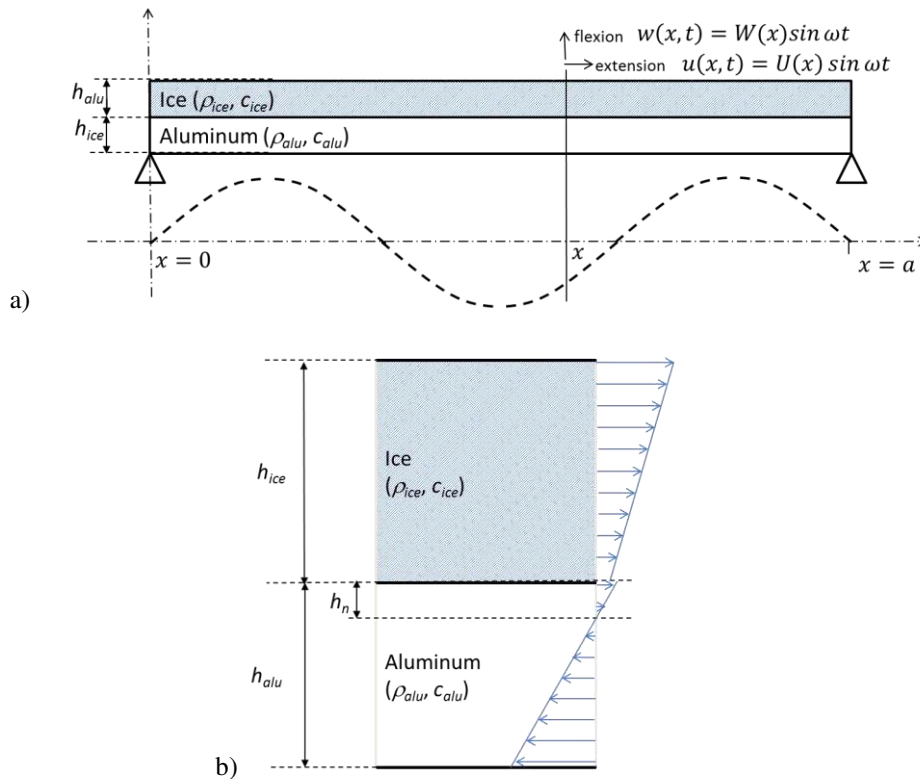

Figure 4 –Element of the beam under study

For flexural modes, the position of the neutral line h_n can be obtained by assuming that the tensile force in a section is zero. This results in:

$$h_n = \frac{1}{2} \frac{c_{alu} h_{alu}^2 - c_{ice} h_{ice}^2}{c_{alu} h_{alu} + c_{ice} h_{ice}} \tag{1}$$

Table 5 synthetizes the analytical equations derived from [29] to compute strains and stresses in the ice, in the aluminum substrate and at the ice-substrate interface. The equations of the peak out-of-plane shear stress were obtained by isolating an element of ice of thickness dx subjected to elastic forces, inertial forces and shear forces at the ice-substrate interface. The resonance frequencies were obtained by the Rayleigh method [30] using the expression of the strains to estimate the kinetic and potential energies.

	Extensional modes	Flexural modes
Displacement	$u(x,t) = U(x) \sin \omega t = U_0 \sin \frac{n\pi x}{a} \sin \omega t$	$w(x,t) = W(x) \sin \omega t = W_0 \sin \frac{n\pi x}{a} \sin \omega t$
		$u(x,t) = -z \frac{\partial w}{\partial x} = U(x) \sin \omega t$
Peak tensile strain	$\varepsilon_x = \frac{\partial U(x)}{\partial x} = U_0 \frac{n\pi}{a} \cos \frac{n\pi x}{a}$	$\varepsilon_x = \frac{\partial U(x)}{\partial x} = W_0 z \left(\frac{n\pi}{a}\right)^2 \sin \frac{n\pi x}{a}$
Peak ice tensile stress in ice	$\sigma_x = c_{ice} \varepsilon_x = c_{ice} U_0 \frac{n\pi}{a} \cos \frac{n\pi x}{a}$	$\sigma_x = c_{ice} (h_{ice} + h_n) \left(\frac{n\pi}{a}\right)^2 W_0 \sin \frac{n\pi x}{a}$
Peak tensile stress in aluminum	$\sigma_x = c_{alu} \varepsilon_x = c_{ice} U_0 \frac{n\pi}{a} \cos \frac{n\pi x}{a}$	$\sigma_x = c_{alu} (h_{alu} - h_n) \left(\frac{n\pi}{a}\right)^2 W_0 \sin \frac{n\pi x}{a}$
Peak out-of-plane shear stress at the ice/aluminum interface	$\tau_{xz} = \left(\rho_{ice} \omega^2 - c_{ice} \left(\frac{n\pi}{a}\right)^2\right) h_{ice} U_0 \sin \frac{n\pi x}{a}$	$\tau_{xz} = c_{alu} \left(\frac{n\pi}{a}\right)^3 \frac{(h_{alu} - h_n)^2 - h_n^2}{2} W_0 \cos \frac{n\pi x}{a}$

Angular frequency	$\omega = \pi \dfrac{n}{a} \sqrt{\dfrac{c_{ice}h_{ice} + c_{alu}h_{alu}}{\rho_{ice}h_{ice} + \rho_{alu}h_{alu}}}$	$\omega = \pi^2 \left(\dfrac{n}{a}\right)^2 \sqrt{\dfrac{EI}{\rho_{ice}h_{ice} + \rho_{alu}h_{alu}}}$ with $EI = \dfrac{c_{alu}}{3}(h_n^3 + (h_{alu} - h_n)^3)$ $+ \dfrac{c_{ice}}{3}((h_n + h_{ice})^3 - h_n^3)$

Table 5 – 1D modes equations

These analytical equations show that:

- for extensional modes, the maximum tensile stress in the substrate or the ice is located on the displacement nodes and the maximum out-of-plane shear stress at the ice-substrate interface is located on the displacement antinodes,
- for flexural modes, the maximum out-of-plane shear stress is located on the displacement nodes.

Figure 5 also compares the extensional and flexural modes, particularly their ability to generate shear stress at the ice-substrate interface. It also gives the tensile stress in the ice and in the aluminum substrate. It shows that, for a given frequency and for a given displacement, the shear stress level at the ice-substrate interface is smaller for extensional than for flexural modes, while the tensile stress in the aluminum substrate is almost the same. Thus, to generate ice delamination while minimizing the displacement of the piezoelectric actuators, it is more interesting to excite flexural modes. This is done for example by architecture *a* of Figure 1. Another conclusion that can be drawn from Figure 5 is that it is more favorable to work at high frequencies: the higher the frequency, the higher the shear stress. However, the frequency of use may be limited by other criteria such as power supply issues.

Note: the results of Figure 5 were obtained for a 2 mm thick ice layer. The expression of out-of-plane shear stress τ_{xz} shows that this stress would be maximum for a null position of the neutral line ($h_n = 0$), which implies an optimal ice thickness h_{ice}:

$$h_{ice} = h_{alu} \sqrt{\frac{c_{alu}}{c_{ice}}} \tag{2}$$

Relation (2) gives an optimal ice thickness of 4.5 mm for a 1.5 mm thick aluminum substrate. However, for future calculations we chose a 2 mm thick ice layer, less attractive in terms of stress generation, but more realistic for the targeted application (de-icing of aircraft flight control surfaces).
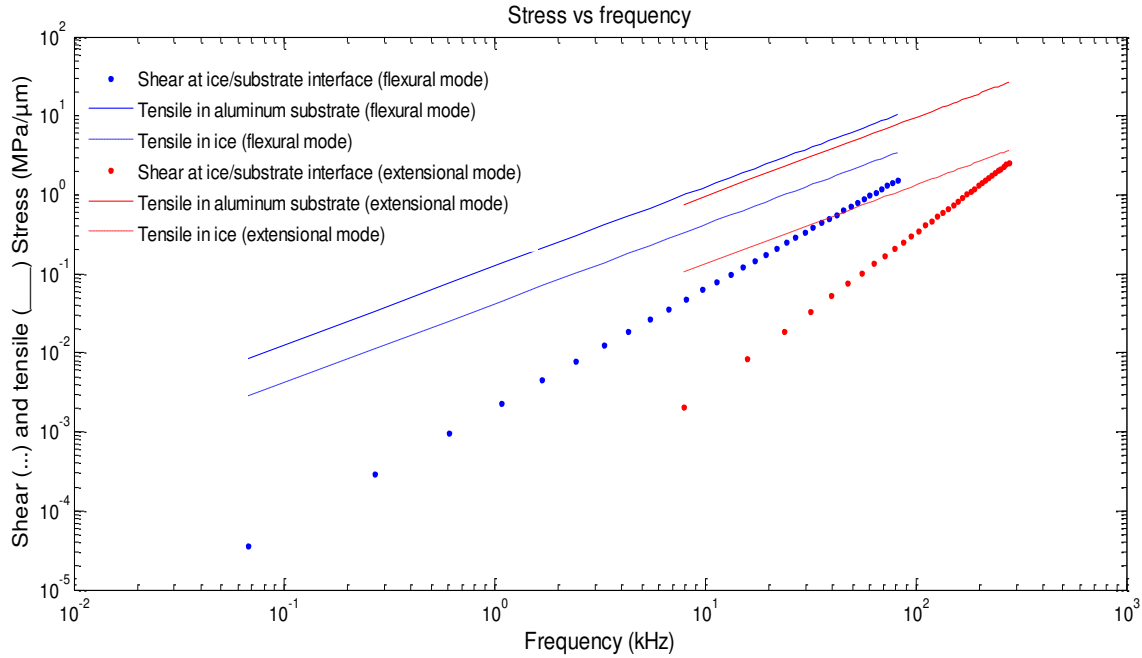

Figure 5 – Comparison of extensional and flexural modes

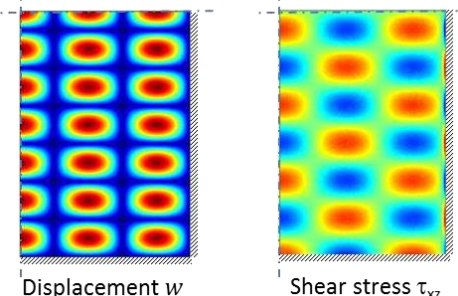## 2.4. Shear stress estimation on 2D models for flexural modes

The previous section gave 1D models of beam type structures. In this section, stresses are expressed for 2D plate type geometries. Following the conclusions of the study for 1D models, stresses will be computed only for flexural modes. For this type of movement, each point of the plate is considered to have a vertical displacement ww in its x and y directions such that $w = $w = w(x, y, t)$. We assume that the displacement $w(x, y, t)$ can be approximated by the analytical solution for flexural modes of a homogeneous plate [30]. Table 6 synthetizes the analytical equations to compute the strains, the shear stress at the ice-substrate interface and the tensile stresses in the aluminum substrate and in the ice. n is the number of anti-nodes on the length for the considered mode and m the number of anti-nodes on the width.

	Flexural modes
Displacements	$w(x, y, t) = W_0 \sin\dfrac{n\pi x}{a} \sin\dfrac{m\pi y}{b} \sin\omega t$ $u(x, y, t) = -z\dfrac{\partial w}{\partial x}$ $v(x, y, t) = -z\dfrac{\partial w}{\partial y}$
Strains	
Peak tensile strain (Sxx)	$\varepsilon_x = W_0 z \left(\dfrac{n\pi}{a}\right)^2 \sin\dfrac{n\pi x}{a} \sin\dfrac{m\pi y}{b}$ $\varepsilon_y = W_0 z \left(\dfrac{m\pi}{b}\right)^2 \sin\dfrac{n\pi x}{a} \sin\dfrac{m\pi y}{b}$
Peak in-plane shear strain (Sxy)	$\gamma_{xy} = \dfrac{1}{2}\left(\dfrac{\partial u}{\partial y} + \dfrac{\partial v}{\partial x}\right) = -z\dfrac{\partial^2 w}{\partial x \partial y} = -zW_0 \dfrac{n\pi}{a}\dfrac{m\pi}{b} \cos\dfrac{n\pi x}{a} \cos\dfrac{m\pi y}{b}$
Stresses	
Peak ice tensile stress (Txx)	$\sigma_x = \dfrac{c_{ice}}{1 - \nu_{ice}^2}(h_{ice} + h_n)\left(\left(\dfrac{n\pi}{a}\right)^2 + \nu\left(\dfrac{m\pi}{b}\right)^2\right) W_0 \sin\dfrac{n\pi x}{a} \sin\dfrac{m\pi y}{b}$
Peak aluminum tensile stress (Txx)	$\sigma_x = \dfrac{-c_{alu}}{1 - \nu_{alu}^2}(h_{alu} - h_n)\left(\left(\dfrac{n\pi}{a}\right)^2 + \nu\left(\dfrac{m\pi}{b}\right)^2\right) W_0 \sin\dfrac{n\pi x}{a} \sin\dfrac{m\pi y}{b}$
Peak in-plane shear stress (Txy)	$\tau_{xy} = -(h_{ice} + h_n)\dfrac{c_{ice}}{1 + \nu_{ice}} W_0 \dfrac{n\pi}{a}\dfrac{m\pi}{b} \cos\dfrac{n\pi x}{a} \cos\dfrac{m\pi y}{b}$
Peak out-of-plane shear stress (Txz)	$\tau_{xz} = \dfrac{c}{1 - \nu^2}\left(\left(\dfrac{n\pi}{a}\right)^2 + (2 - \nu)\left(\dfrac{m\pi}{b}\right)^2\right)\dfrac{n\pi}{a}\dfrac{(h_{alu} - h_n)^2 - h_n^2}{2} W_0 \cos\dfrac{n\pi x}{a} \sin\dfrac{m\pi y}{b}$

Table 6 – 2D flexural modes equations

These equations are validated by a Finite Element analysis performed for the geometry of the study case (h_{alu} = 1.5 mm, c_{alu} = 70 GPa, h_{ice} = 2 mm, c_{ice} = 9.7 GPa, h_n = 0.48 mm, a=290 mm, b = 200 mm). Table 7 shows the mode for n=13

and m=5 of frequencies around 15 kHz, which is an intermediate frequency among the frequencies usually used for tests with piezoelectric ceramics bonded on substrate. The comparison of analytical and numerical results shows a difference of less than 8% and validates the analytical models developed.

Flexural mode n=13 m=5	 Displacement w	 Shear stress τ_{xz}
	Analytical results	Numerical results
Resonance frequency	15554 Hz	14732 Hz
Maximum tensile stress in the ice layer	0.57 MPa/µm	0.52 MPa/µm
Maximum shear stress at the ice/substrate interface	0.134 MPa/ µm	0.144 MPa/µm

Table 7 – Comparison of analytical equations and Finite Element Analysis

2.5. Frequency range for piezoelectric de-icing systems

The equations of Table 6 will be used to study the feasibility of de-icing systems with piezoelectric actuators and to highlight the frequency ranges leading to efficient piezoelectric deicing devices. The study will be performed for the study case of section 2.1, with a number of anti-nodes in the length varying between 1 and 25 and a number of anti-nodes in the width varying between 1 and 15.

Figure 6 and Figure 7 show that the shear stress per µm of displacement at the ice/substrate interface and the tensile stress per µm in aluminum or ice increase with the number of anti-nodes and with frequency. One requirement for de-icing systems is to remove ice without stressing the structure on which it is deposited. This means that de-icing systems must maximize stress at the ice/substrate interface while minimizing stress in the structure. The ratio of tensile stress in aluminum to shear stress at the ice/substrate interface represented in Figure 8 allows the frequency range to be found for

which the de-icing systems are the most efficient in meeting this requirement and shows that ultrasonic frequencies, higher than 20 kHz, are more favorable.
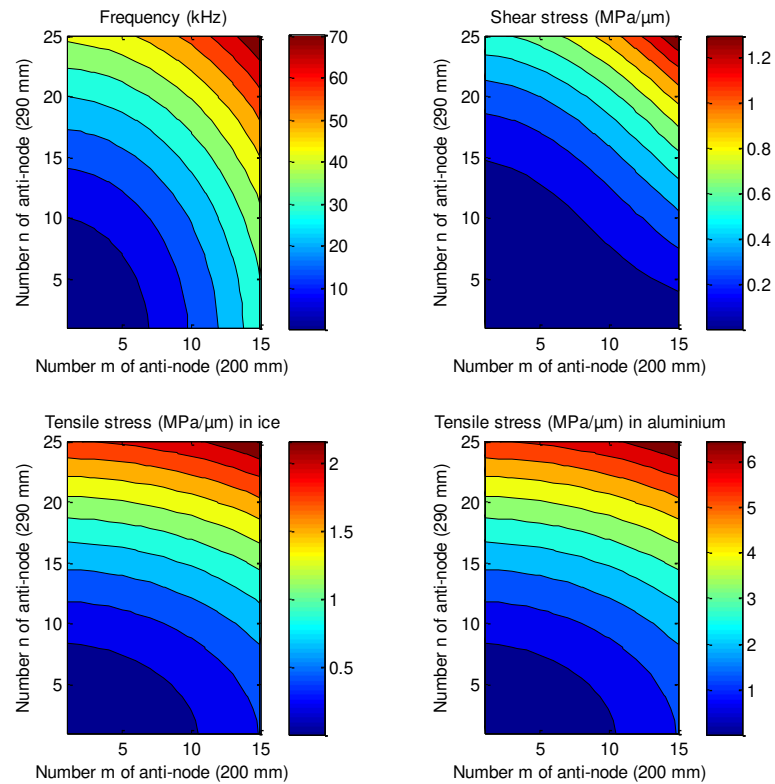

Figure 6 - Flexural resonance frequencies and stresses for the study case versus the number of anti-nodes
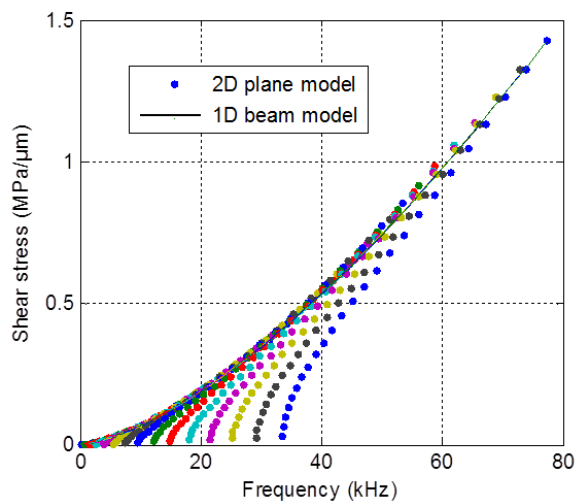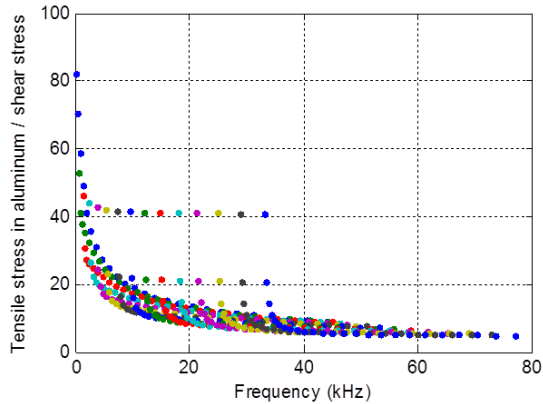

Figure 7 - Shear stress per µm according to frequency for flexural modes

Figure 8 - Aluminum stress / shear stress according to frequency for flexural modes

3. EVALUATION OF DIFFERENT ARCHITECTURES OF PIEZOLECTRIC DE-ICING SYSTEMS

The previous section highlighted the type of modes (flexural modes) and the frequency range (ultrasonic) of the resonant modes to be excited to lead to ice delamination. This section aims to assess the type of piezoelectric actuators to be used. Two kinds of actuators are compared: patch type actuators, directly bonded on to the structure to be activated, and Langevin pre-stressed actuators in the configuration Figure 1a.

3.1. Methodology for evaluating piezoelectric deicing systems

The proposed methodology for evaluating the 2 different architectures of piezoelectric de-icing systems is divided into 2 main phases:

1. Computation of a reduced model (analytically or numerically) of the chosen architecture of the de-icing system connected to the surface with the layer of ice. Computation of the maximal tensile stress per µm within the PZT ceramics and of the shear stress per µm at the ice/substrate interface. All these results are computed for the resonance mode for which the coupling between the piezoelectric actuator and the structure is the best, i.e. for which the required voltage will be the lowest.

2. Computation of the displacement required to generate the minimal stress value and of the voltage that leads to the required displacement. As the piezoelectric de-icing systems are resonant systems, this result depends strongly on the damping of the structure with the ice.

3.1.1. *Reduced model of systems with piezoelectric actuators*

This section details the computations of the two design methodology phases. These details are extracted from [34]. The reduced model of a structure with piezoelectric actuators can be made for one mode with a mechanical equation and an electrical equation:

$$\begin{cases} M\ddot{q} + D_s\dot{q} + Kq = NV \\ q_C = Nq + C_oV \end{cases} \tag{3}$$

where q is the modal displacement, M the modal mass, K the modal stiffness, q_c the electrical charge, V the voltage, D_s the modal damping, N the modal electromechanical coupling factor, and C_o the modal turned-off capacity.

This model can be computed analytically for simple geometries or with multiphysics Finite Element software (such as COMSOL©, ANSYS© or ABAQUS©) that allows calculations with piezoelectric elements. If the computations are carried out with short-circuited piezoelectric patches, $V=0$ and the equations become:

$$\begin{cases} M\ddot{q} + D_s\dot{q} + Kq = NV \\ q_C = \theta q \end{cases} \tag{4}$$

which means that

$$N = \frac{q_c}{q} \tag{5}$$

and for the resonance:

$$N = \frac{q_c}{q} \tag{6}$$

For structures with low damping,

$$Q_m \approx \frac{K}{\omega D_s} \tag{7}$$

Consequently, if the displacement required to de-bond ice is known for a resonance mode, the voltage that generates this displacement is given by:

$$Q_m \approx \frac{K}{\omega D_s} \tag{8}$$

3.1.2. Design drivers of piezoelectric actuators

The electromechanical coupling factor N describes the ability of the piezoelectric actuators to generate a force on the degree of freedom q for a given resonance mode. Moreover, stresses are proportional to displacements of the degrees of freedom. We chose to compute the electromechanical coupling factor for the point characterized by the largest displacement (in-plane or out-of-plane depending on excited modes). The electromechanical coupling factor may be influenced by: the mode of the piezoelectric ceramic of the transducer (mode 31 for the bonded patch and mode 33 for the Langevin transducer), the dimensions and positioning of the ceramic relative to the nodes and antinodes, and the presence of adhesive.

A piezoelectric transducer may have several operational limits [35]: maximum voltage to avoid depolarization by application of an excessive electric field (400 V/mm of ceramic thickness), maximum stress in the ceramics to avoid failure (about 24 MPa in extension for dynamic applications and for non-pre-stressed ceramics) and maximum temperature to avoid reaching the Curie temperature, which leads to depolarization. The thermal limit will not be considered here because of the very low ambient temperatures.

As shown in Equation 30, the displacement at resonance depends on the damping of the structure, characterized by a mechanical quality coefficient. This coefficient is highly dependent on the boundary conditions and on the complexity of the assembly. To assess the different architectures, we assume a value of Q_m equal to 100 here, which corresponds to a damping coefficient of 0.5%.

3.2. Piezoelectric de-icing system with bonded ceramics

The first configurations studied here are inspired directly from the work of Palacios ([17][18][20][21]) because he experimentally proved their ability to provide instantaneous de-icing even for untreated surfaces (without polishing, without hydrophobic or icephobic coating). The actuator configurations consist of one or more PZT disks glued onto the surface to be de-iced. Palacios explained that ice delamination occurs for frequencies near the first radial extensional mode of the piezoelectric disk.

Two simple configurations will be processed in this section:

- Free axisymmetric disks described in [36] (Figure 9a). This study, which allows simple 2D Finite Element analyses because of the symmetry, will help the phenomena involved to be understood on a 2D model and allows the parameters that are negligible for future simulations in 3D (e.g. glue thickness) to be estimated, thus avoiding fine meshes of very thin layers and heavy 3D models.

- Clamped plates with the dimensions given in section 2.1 (Figure 9b). This geometry will allow a comparison with the architecture based on a Langevin transducer, which will be studied in the next section. A volume of ceramic similar to that of the Langevin transducer is chosen in order not to bias the comparison.

(a)　　　(b)
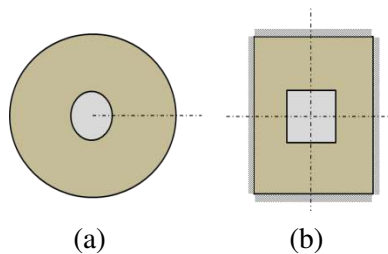
Figure 9 - Studied configurations with bonded ceramics (free disk and clamped plate)

We start by the study of the free axisymmetric disks. Figure 10 describes the geometry studied by Soltis under the direction of Palacios [36]. We performed studies step by step (PZT ceramic only, aluminum plate only, PZT/aluminum plate, PZT/aluminum plate /ice) to understand the principle of ice delamination.
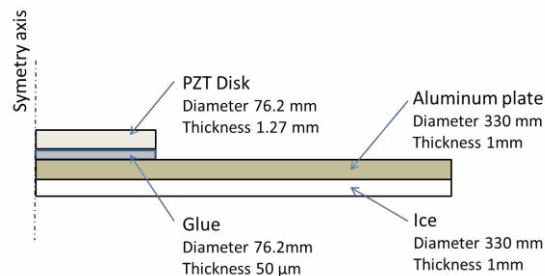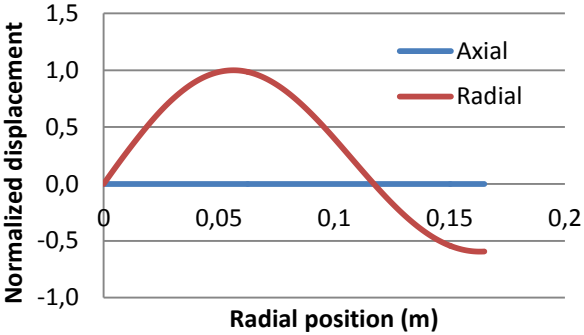

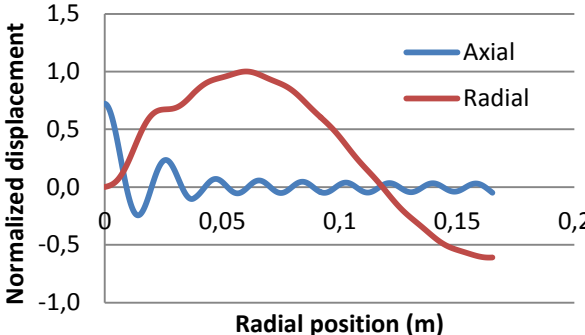**Figure 10 - Axisymmetric configuration with bonded ceramics (disk)**

The study of the piezoelectric ceramic alone shows that the extensional radial frequency of the PZT disk is around 29.9 kHz. As Palacios recommends studying the modes around the extensional radial mode of the PZT disk, extensional and flexural modes around this frequency are preferentially studied.

We first look at the modal shape of these 2 modes. Figure 11(a)(b)(c) shows the modal shapes of the aluminum plate alone (case (a)), the aluminum plate with the piezoelectric disk (case (b)) and the aluminum plate with the piezoelectric disk and ice (case (c)). These modal shapes are represented for the extensional radial frequency close to that of the PZT disk. With a PZT disk bonded on the aluminum plate (with or without ice), the configuration is not symmetric about one plane normal to the axisymmetric axis and the radial mode thus generates both radial and axial displacements. Figure 11(d) shows the modal shape of the flexural frequency close the extensional radial frequency of the PZT disk for the case of aluminum plate with piezoelectric disk and ice. The axial displacements generated by the flexural mode are phased-shifted by a quarter of a wavelength compared to the axial displacements generated by the extensional mode. Such axial displacements generated by the flexural and extensional modes and phased-shifted explain why this configuration excited by a sweep in frequency is favorable to de-ice the entire surface: nodes of the axial displacements for which shear stress are important are spread over the entire surface.

Then Table 8 gives (i) the parameters of the reduced model for the flexural and extensional modes, including the electromechanical force factor, and (ii) the computation results of the shear stresses required to de-bond the ice. The extensional mode has a high electromechanical force factor; the transducer is well-coupled with the structure. For a quality factor of 100, the required displacement to de-bond the ice is 9.22µm, which induces a voltage of 124 V - which is reasonable - and a tensile stress in the aluminum plate of nearly 42 MPa – which is quite high. For the flexural mode, the electromechanical force factor is much smaller but, as the stiffness is also smaller, the required displacement to de-bond the ice is 7.72µm and the required voltage is 88 V. The tensile stress in the aluminum plate is also around 42 MPa, similar to the extensional mode.
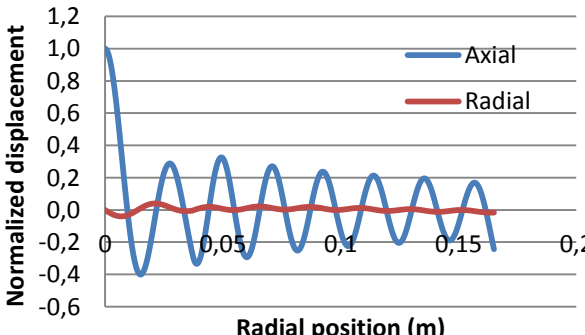
(a) Extensional mode for Alu (28 kHz)

(b) Extensional mode for Alu+PZT (28.5 kHz)
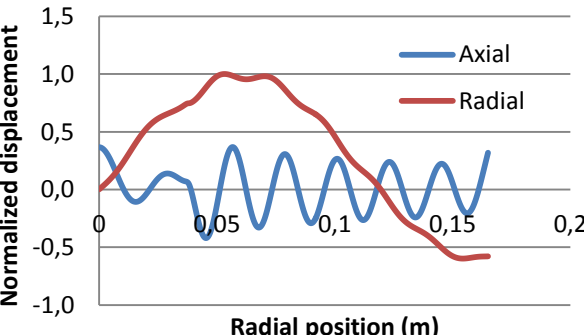
(c) Extensional mode for Alu+PZT+Ice (26.2 kHz)

(d) Flexural mode for Alu+PZT+Ice (27.7 kHz)

Figure 11 – Axial and radial displacements for axisymmetric configuration
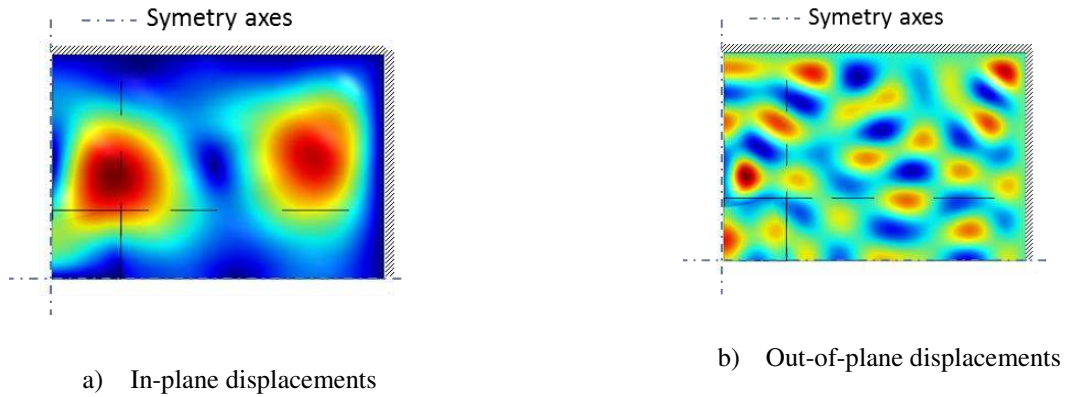
Computed electromechanical parameters of the reduced model and stresses per µm (results of Finite Element Analysis)				
			Extensional mode at 26.2 kHz	Flexural mode at 27.2 kHz
Modal mass	M	Kg	0.12	0.01
Modal stiffness	K	N/m	3.18E+09	3.74E+08
Modal electromechanical coupling factor	N	N/V	2.37	0.33
Shear stress xz /µm at ice/substrate interface	$T_{xz}/\mu m$	MPa/µm	0.11	0.13
Tensile stress xx /µm in PZT	$T_{xx}/\mu m$	MPa/µm	4.55	5.45
Ratio Txx/Txz		-	41.95	42.07
Displacements and voltages required to de-bond the ice				
Shear stress required to de-bond ice	T_{xz}	MPa	1	1
Displacement required to de-bond ice	U_o	µm	9.22	7.72
Tensile stress in PZT	$T_{xx\ PZT}$	MPa	41.95	42.07
Quality factor	Q_m	-	100	100
Voltage supply	U	V	124	88

Table 8 – Computation results for the axisymmetric configuration

in the case of bonded PZT+Aluminum Plate+Ice

The next study is the study case (see section 2.1) of this article: a rectangular aluminum plate of dimensions 290x200x1.5 mm³. We consider a square piezoelectric ceramic of dimensions 60x60x2.5 mm³ bonded in the center of the plate, the volume of which is similar to that of the bolt-clamped transducer that will be used in the next section. The extensional radial frequency of the PZT ceramic is around 31.8 kHz. The resonance extensional frequency of the aluminum plate/ice/PZT assembly close to that frequency is 33.2 kHz. For this extensional frequency, Figure 12 shows the in-plane and out-of-plane displacements. In-plane magnitudes are 5.6 times higher than out-of-plane magnitudes. The computed

electromechanical force factor is 1.2 N/V. Obtaining sufficient stresses to achieve delamination requires a voltage of about 86 V and also displacement of 21 µm, which generates a very high stress level in the piezoelectric ceramic. Palacios emphasizes this issue, which leads to the breakdown of ceramics, in numerous works ([36],[37]).

a) In-plane displacements

b) Out-of-plane displacements

Figure 12 – Displacements for the extensional frequency (33.20 kHz) close to radial frequency of the ceramic (rectangular configuration with a bonded piezoelectric ceramic)

Computed electromechanical parameters of the reduced model and stresses per µm (results of Finite Element Analysis)			
			Extensional mode at 33.2 kHz
Modal mass	M	Kg	0.01
Modal stiffness	K	N/m	4.90E+08
Modal electromechanical coupling factor	N	N/V	1.2
Shear stress xz /µm at ice/substratum interface	Txz/µm	MPa/µm	0.05
Tensile stress xx /µm in PZT	Txx/µm	MPa/µm	3.33
Ratio Txx/Txz		-	70
Displacements and voltages required to de-bond ice			
Shear stress required to de-bond ice	Txz	MPa	1
Displacement required to de-bond ice	U_0	µm	21
Tensile stress in PZT	$T_{xx\,PZT}$	MPa	70

Quality factor	Q_m	-	100
Voltage supply	U	V	86

Table 9 – Computation results for the rectangular configuration

in the case of bonded piezoelectric ceramic+aluminum plate+ice

3.3. Piezoelectric de-icing system with Langevin transducers

In order to excite flexural modes of the surfaces to be protected, the architecture of Figure 1(a) is studied here. A bolt-clamped Langevin transducer (Figure 13) is thus connected to the plate described in section 2.1 through a spacer ring of length 10 mm. The extensional resonance frequency of the transducer alone is 40.44 kHz. For the Langevin transducer/aluminum plate/ice assembly, the resonance frequency for which the delamination of the ice occurs with the lowest supply voltage is 46.857 kHz. For that frequency, the electromechanical force factor is 1.25 N/V. Obtaining sufficient shear stresses to achieve delamination requires a voltage of about 123 V and the tensile stress in the piezoelectric ceramics is then 9.8 MPa, which is much less than for architectures with bonded piezoelectric ceramics.

Figure 13 - Bolt-clamped Langevin transducer and its first extensional resonance mode

Figure 14 – Study case: bolt-clamped Langevin transducer connected to the plate

a) Out-of-plane displacements

b) Shear stress at the ice/substrate interface

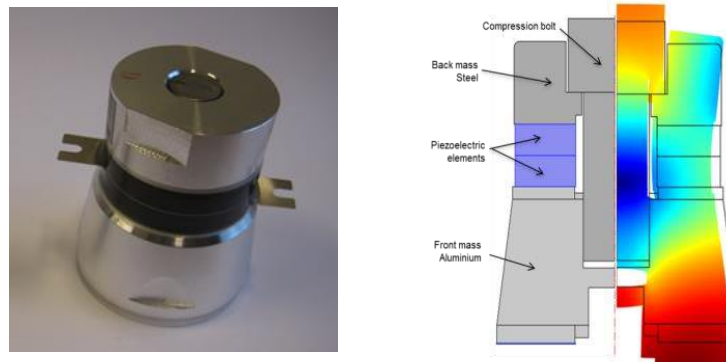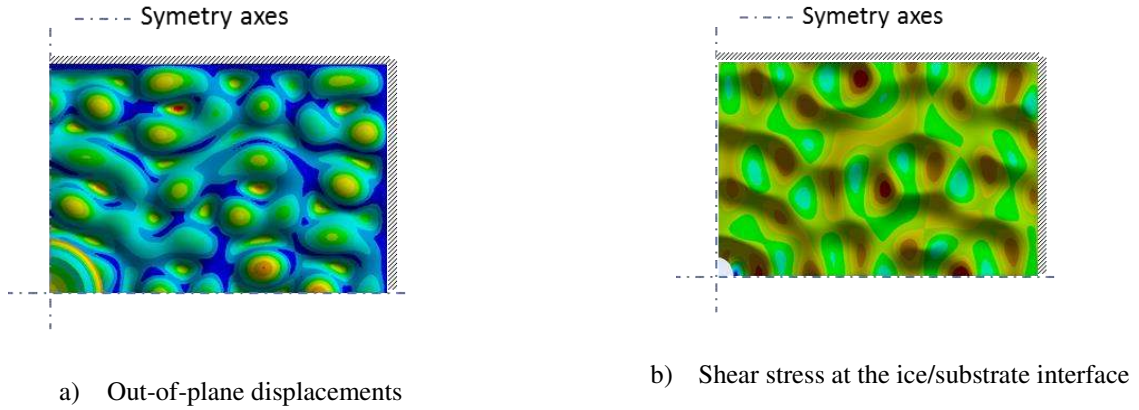**Figure 15 – Displacements for the flexural mode (46.86 kHz) (rectangular configuration with a Langevin**

transducer)

Computed electromechanical parameters of the reduced model and stresses per µm (results of Finite Element Analysis)			
			Results at 46.857 kHz
Modal mass	M	Kg	0.0096
Modal stiffness	K	N/m	8.4e+09
Modal electromechanical coupling factor	N	N/V	1.25
Shear stress xz /µm at ice/substrate interface	$T_{xz}/\mu m$	MPa/µm	0.55
Tensile stress xx /µm in PZT	$T_{xx}/\mu m$	MPa/µm	5.3
Ratio Txx/Txz		-	9.63
Displacements and voltages required to de-bond ice			
Shear stress required to de-bond ice	T_{xz}	MPa	1
Displacement required to de-bond ice	W_0	µm	1.83
Tensile stress in PZT	$T_{xx\ PZT}$	MPa	9.8
Quality factor	Q_m	-	100
Voltage supply	U	V	123

Table 10 – Computation results for the rectangular configuration

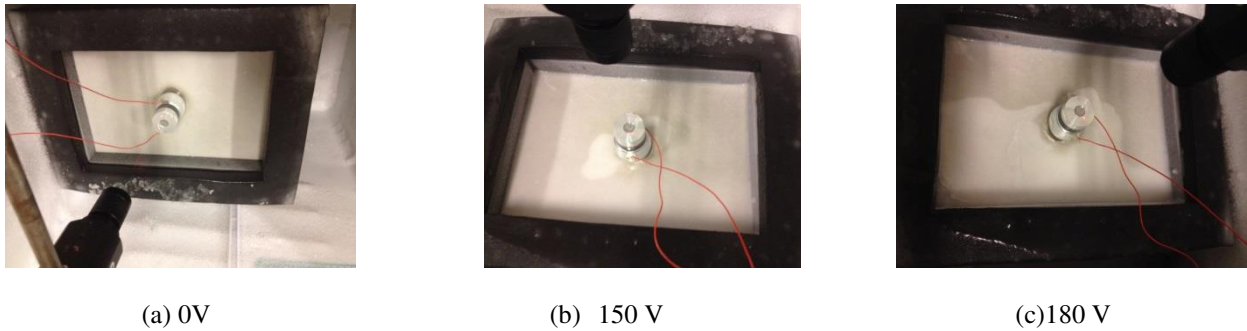**in the case of Langevin transducer+spacer+aluminum plate+ice**

3.4. Comparison of the 2 architectures

It is possible to compare the actuating architectures according to several criteria:

- The limitations of use owing to stresses in PZT ceramics. The advantage of the architecture with Langevin transducers is that stresses in the ceramics are only 9.8 MPa, which is 7 times less than for the architecture with bonded ceramics. Moreover, the risk of mechanical failure is much lower for Langevin transducers than for bonded ceramics as their pre-stressed structure enables them to withstand higher stresses in operation.

- Power consumption is mainly due to mechanical losses during resonance and thus to the mechanical energy of elastic deformation. This energy is 7.8 times greater for the architecture with bonded ceramics because it requires much greater deformations (21 microns against 1.83 microns).

- The size of the power electronics is dependent on the power consumption but also on the capacitive energy stored in PZT ceramics. Power devices with good efficiency, such as resonant inverters, have inductors which are all the larger when the capacitive energy is high. This energy is 2.2 times greater for the architecture with bonded ceramics because, even if the voltage is lower, the capacitance is greater.

3.5. Experimental validation

Tests were performed on the solution with the Langevin transducer, which seems the most promising if we consider a criterion that minimizes the energies involved and the stresses in the piezoelectric ceramics. A clamped aluminum plate without coating was covered with 2 mm of ice (glaze-type ice obtained in a freezing chamber). The Langevin transducer was then supplied with a voltage of around 46kHz frequency and 150V and 180V amplitude. Figure 16 shows the results achieved during the experiment. The delamination of the ice started to occur at 150 V and was even more visible at 180 V. The difference between the estimated voltage and the voltage measured during the experiment may come from the uncertainty on the quality factor, the non-linearity and the uncertainties on the shear stress leading to ice delamination (assumed to 1 MPa for computations).

(a) 0V　　　　　　　　　　(b)　150 V　　　　　　　　　(c)180 V

Figure 16 – Experimental results for the configuration Langevin transducer+spacer+aluminum plate+ice and excitation of the flexural mode of 46.86 kHz frequency

4. CONCLUSION

This article has aimed to compare different architectures of de-icing systems based on piezoelectric actuators and on the use of structural resonance modes. The analytical models of the aluminum substrate with ice have shown that it is more interesting to excite flexural modes than extensional modes to maximize the shear stress at the substrate/ice interface. These models also highlighted that ultrasonic frequencies over 20 kHz allowed the shear stress to be maximized for a given displacement, thus avoiding fatigue in the substrate and limiting breakdown of the actuators. The modeling of the substrate and the actuators by finite element models highlighted the interest of Langevin type actuators with regard to the resistance to mechanical stress and the mechanical and electrical energies involved in this kind of de-icing system. Tests validated the efficiency of ice delamination with an architecture based on Langevin type actuators and favoring structural flexural modes. These experiments also confirm the interest of studying such solutions more intensively.

5. REFERENCES

[1]   Civil Aviation Authority. Aircraft Icing Handbook, 2000

[2]   Z. Goraj, An overview of the deicing and anti-icing technologies with prospects for the future, 24th Congress of International Council of the Aeronautical Sciences, 29 August-3 September, Yokohama, Japan, 2004

[3]   Federal Aviation Administration. Advisory Circular AC 91-74A - Pilot Guide: Flight in Icing Conditions, 2007

[4]   O. Meier, D. Schloz, A handbook method for the estimation of power requirements for electrical de-icing systems, DLRK, Hamburg, 2010

[5]   D. Kevin, L.B. Murphy, Aircraft deicing and anti-icing equipment, Safety Advisor, AOPA Air Safety Advisor Wheather, Vol.2, pp.1-10, 2004

[6]   R. Myose, W. Horn, Y. Hwang, J. Herrero et al., Application of Shape Memory Alloys for Leading Edge Deicing, SAE Technical Paper 1999-01-1585, 1999, doi:10.4271/1999-01-1585.

[7]   S. Ramanathan; V.V. Varadhan, V.K. Varadhan, De-Icing of Helicopter Blades Using Piezoelectric Actuators, Smart Structures and Materials, Smart Electronics and MEMS, 281 (June 21, 2000), pp. 354-363, 2000

[8]   M.K. Kalkowski; T.P. Waters, E. Rustighi, Removing surface accretions with piezo-excited high-frequency structural waves, Proc. SPIE 9431, Active and Passive Smart Structures and Integrated Systems 2015, San Diego, California, United States, March 08, 2015

[9]   S.V. Venna, Y.J. Lin, In-Flight De-Icing Self-Actuating Wing Structures with Piezoelectric Actuators, Proceedings of American Society of Mechanical Engineers/International Mechanical Engineering Congress and Exposition 2002, ASME Press, New York, NY, pp. 237–245., 2002

[10] S.V. Venna, Y.J. Lin, Development of Self-Actuating In-Flight De-Icing Structures with Power Consumption Considerations, Proceedings of the American Society of Mechanical Engineers International Mechanical Engineering Congress and Exposition 2003, ASME Press, New York, NY, pp. 45–53, 2003

[11] S.V. Venna, Y.J. Lin, Mechatronic development of self-actuating in-flight deicing systems, IEEE/ASME Transactions on Mechatronics, vol.11(5), pp.585-592, 2006

[12] S.V. Venna, Y.J. Lin, G. Botura, Piezoelectric Transducer Actuated Leading Edge De-Icing with Simultaneous Shear and Impulse Forces, Journal of Aircraft, Vol. 44, pp.509-515, 2007

[13] J. Palacios, E. Smith, J. Rose, R. Royer, Instantaneous De-Icing of Freezer Ice via Ultrasonic Actuation, AIAA journal, vol. 49(6), 1158-1167.

[14] S. Struggl, J. Korak, C. Feyrer, A basic approach for wing leading deicing by smart structures, Sensors and Smart Structures Technologies for Civil, Mechanical, and Aerospace Systems, Vol. 7981, 2011

[15] R. Seppings, Investigation of Ice Removal From Cooled Metal Surfaces, Mechanical Engineering Department, Imperial College London, 2006

[16] J.L. Palacios, Design, Fabrication, and Testing of an Ultrasonic De-Icing System for Helicopter Rotor blades, PhD Thesis, The Pennsylvania State University, Department of Aerospace, May 2008

[17] J.L. Palacios, E.C. Smith, J. Rose, Investigation of An Ultrasonic Ice Protection System For Helicopter Rotor Blades, Annual Forum Proceedings - AHS International 64th Annual Forum, Vol. 1, pp. 609-618, 2008

[18] J.L. Palacios, E.C. Smith, J. Rose, R. Royer, Ultrasonic De-Icing of Wind Tunnel Impact Icing, Journal of Aircraft, Vol. 48(3), pp. 1020- 1027, 2011

[19] J.L. Palacios, E.C. Smith, Dynamic Analysis and Experimental Testing of Thin-Walled Structures Driven by Shear Tube Actuators, AIAA 46th AIAA/ASME/ASCE/AHS/ASC Structures, Structural Dynamics and Materials Conference, 18 April-21 April, 2005

[20] A. Overmeyer, J. Palacios, E. Smith, R. Royer, Rotating Testing of a Low-Power, Non-Thermal Ultrasonic De-icing System for Helicopter Rotor Blades, SAE Technical Paper, International Conference on Aircraft and Engine Icing and Ground Deicing, June 13-17 2011, Chicago, IL 2011

[21] A. Overmeyer, J. Palacios, E. Smith, Actuator Bonding Optimization and System Control of a Rotor Blade Ultrasonic Deicing System, 53rd AIAA/ASME/ASCE/AHS/ASC Structures, Structural Dynamics and Materials Conference, 23 April-26 April, 2012

[22] S. Tarquini, C. Antonini, A. Amirfazli, M. Marengo, J. Palacios, Investigation of ice shedding properties of superhydrophobic coatings on helicopter blades, Journal of Cold Regions Science and Technology, Vol. 100 , pp. 50–58, 2014

[23] T. Strobl, S. Storm, M. Kolb, J. Haag, M. Hornung, Development of a Hybrid Ice Protection System based on Nanostructured Hydrophobic Surfaces, ICAS Conference, St. Petersburg, Russia, 7-12 September, 2014

[24] J.J. Petrovic, Mechanical Properties of Ice and Snow, Journal of Material Science, Vol. 38, 2003.

[25] R.J. Scavuzzo, M. L. Chu, Structural Properties of Impact Ices Accreted on Aircraft Structures, NASA Contractor Report 179580, 1987

[26] HH. G Jellinek, Adhesive Properties of Ice – Part II, 1960

[27] C. Laforte, J. Laforte, Deicing Strains and Stresses of Ice Substrates, Journal of Adhesion Science and Technology 26 (2012) 603-620

[28] D.L Loughborough, E.G. Hass, Reduction of Adhesion of Ice to De-icer Surfaces, Journal of Aeronautical Sciences, Vol.13(3): pp. 126-134, 1946

[29] S. Timoshenko, Strength of Materials, D. Van Nostrand, 1955

[30] M. Géradin, D.J. Rixen, Mechanical vibrations: theory and application to structural dynamics. John Wiley & Sons, 2014

[31] R.D. Blevins, Formulas for Natural Frequency and Mode Shape, 2001.

[32] J.N. Reddy, Mechanics of Laminated Composite Plates and Shells: Theory and Analysis, 2°ed. 2004

[33] J.N. Reddy, Energy and Variational Methods in Applied Mechanics: With an Introduction to the Finite Element Method,1984

[34] V. Pommier-Budinger, M.Budinger, Sizing optimization of piezoelectric smart structures with meta-modeling techniques for dynamic applications, International Journal of Applied Electromagnetics and Mechanics, Vol.46(1), pp.195-206.

[35] D.A. Berlincourt, H.H.A. Krueger, Behaviour of Piezoelectric Ceramics under Various Environmental and Operation Conditions of Radiating Sonar Transducers, Technical Publication TP-228, Morgan Electro-Ceramics.

[36] J.T. Soltis, Design and testing of an erosion resistant ultrasonic de-icing system for rotorcraft blades, Thesis in Aerospace Engineering at Pennsylvania State University, 2013.

[37] A.D. Overmeyer, Actuator bondline optimization and experimental deicing of a rotor blade ultrasonic deicing system, Thesis in Aerospace Engineering at Pennsylvania State University, 2012.